JOURNAL OF MAGNETIC RESONANCE **128,** 21–29 (1997)
ARTICLE NO. MN971206

New Multinuclear Experiments on Solid Organotin Fluorides

Julian C. Cherryman and Robin K. Harris[1]

Department of Chemistry, Science Laboratories, University of Durham, South Road, Durham DH1 3LE, United Kingdom

Received February 5, 1997; revised April 2, 1997

^{n}Bu$_3$SnF and Mes$_3$SnF (Mes = mesityl) are organotin fluorides that have direct Sn–F bonds. The ^{119}Sn and ^{19}F NMR spectra of these compounds have been measured using a selection of CPMAS probes. Doubly decoupled {^{1}H, ^{19}F} as well as singly decoupled {^{1}H} ^{119}Sn NMR spectra are shown. Double decoupling gives higher resolution spectra and allows the sample of Mes$_3$SnF to be spun slower to give more spinning-sidebands without overlapping of signals, giving improved analysis. The doubly decoupled spectra are sensitive to the power and offset of the decouplers. The effect of off-resonance decoupling has been observed for ^{119}Sn NMR through reduced splittings when the ^{19}F decoupler power and offset were varied. Proton-decoupled ^{19}F spectra have been measured using a new HF double-resonance probe. In addition, two-dimensional heteronuclear correlation spectra are presented for Mes$_3$SnF, allowing a full assignment for the ^{19}F and ^{119}Sn chemical shifts of the two sites. Full shielding tensor data are reported for both compounds. Values have been derived for the effective (^{119}Sn, ^{19}F) dipolar coupling constants from both ^{119}Sn and ^{19}F experiments, yielding estimates of coupling anisotropy.

INTRODUCTION

Solid-state ^{119}Sn NMR spectroscopy has been used with many different compounds to give structural and crystallographic information, including shielding tensor components. Tin systems studied include organotin halides (*1*), polymers (*2*), chalcogenides (*3*), and other cyclic and noncyclic organotin compounds (*4*). Tin has three spin-$\frac{1}{2}$ isotopes, of which ^{119}Sn is most commonly used due to its slightly higher magnetic moment and appreciable natural abundance of 8.58%. Tin-119 NMR spectroscopy can be applied to the study of solids using magic-angle spinning (MAS), often together with cross polarization (CP). Its good sensitivity and large chemical shift range (ca. 2500 to −2500 ppm with respect to the signal for Me_4Sn) make it valuable for structure determination. The shielding anisotropy (SA) is often also large, and its size can give an indication of the coordination at the ^{119}Sn center. A recent review of SA for various ^{119}Sn compounds (*5*) has shown that it is very sensitive to the coordination number, with values as large as 1000 ppm for hepta-coordinate centers. In such cases the SA cannot be fully averaged with high-speed MAS.

Of the triorganyltin fluorides, R_3SnF, previous papers have only reported the proton-decoupled ^{119}Sn spectra of the compounds R = Me, ^{i}Bu, ^{n}Bu, Ph and Mes (*6–8*). Detailed work has not been presented on the ^{n}Bu$_3$SnF compound (*6*). Some triorganyltin compounds are known to form linear chains in the solid state, in which the tin center is penta-coordinate. For ^{n}Bu$_3$SnF this can be seen by the isotropic shift and by the triplet splitting in the ^{119}Sn spectra, the latter indicating that there are two equivalent fluorines coupling to each tin atom. With a bulky group such as mesityl (Mes), steric hindrance prevents the close approach of two molecules, and diffraction data have shown that there are two tetra-coordinate molecules in the asymmetric unit.

Recently, using a Chemagnetics triple-channel probe tuned for ^{1}H, ^{19}F, and ^{119}Sn, we have been able to record doubly decoupled ^{119}Sn{^{1}H, ^{19}F} spectra for ^{n}Bu$_3$SnF and Mes$_3$SnF. We believe that this is the first time that ^{119}Sn spectra of this type have been published. The probe allows us to record high-resolution ^{119}Sn spectra with splittings from both proton and fluorine coupling fully removed. Moreover, variable-power fluorine decoupling scales the observed splitting and provides a way to calibrate the real power entering the probe.

Fluorine-19 has 100% natural abundance and is a spin-$\frac{1}{2}$ nucleus. The resonant frequencies of ^{19}F and ^{1}H are only 6% apart, which makes observation of ^{19}F signals while simultaneously applying proton decoupling difficult, and only a few reports are in the literature (*9–14*). However, the HF probe used for the work reported here has an efficient trap between the two channels which, with the use of narrow-pass filters, makes ^{19}F{^{1}H} observation entirely feasible. Indeed cross polarization from ^{1}H to ^{19}F was regularly used for these studies because of the much shorter pulse delay required for ^{1}H relaxation than for ^{19}F.

Here we use the observation of ^{119}Sn{^{1}H}, ^{119}Sn{^{1}H, ^{19}F}, and ^{19}F{^{1}H} spectra for ^{n}Bu$_3$SnF and Mes$_3$SnF to extend the previous spinning-sideband analyses. As the sideband manifolds are split into subspectra by the Sn–F scalar coupling, values for the shielding tensor components and for the effective dipolar coupling constants may be calculated separately (*8*). For this paper we have carried out, for the

[1] To whom correspondence should be addressed. Fax: +44-(0)-191-386-1127. E-mail: r.k.harris@durham.ac.uk.

1090-7807/97 $25.00

first time, a combined fit of the three sets of data to give the three effective anisotropies and hence improved values for the effective dipolar coupling constants. This has been done for $^{n}Bu_3SnF$ using the triplet in the ^{119}Sn spectrum, and the centerband with the $^{117,119}Sn$ satellite doublets in the ^{19}F spectrum. For Mes_3SnF the doubly and singly decoupled ^{119}Sn spectra were used together. It was not possible to obtain the three values for the effective anisotropy by observing ^{19}F directly for Mes_3SnF as the spectrum was too crowded and the satellite peaks too weak. However, a heteronuclear shift correlation (HETCOR) experiment has separated the two sites, allowing an approximate value of the anisotropies to be calculated.

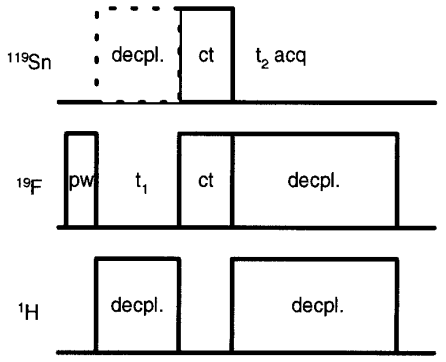

FIG. 1. The heteronuclear correlation pulse sequence used, with optional decoupling during t_1 shown as a dashed pulse. The experiments utilized a phase cycle of length 8 and hypercomplex data acquisition.

EXPERIMENTAL

All NMR spectra were recorded using a Chemagnetics CMX200 Spectrometer with resonant frequencies of ^{1}H, 200.13 MHz; ^{19}F, 188.29 MHz; and ^{119}Sn, 74.63 MHz. A double-channel Chemagnetics HX probe was used for ^{119}Sn observation, with a HFX triple-channel probe for the double-decoupling experiments. Both probes use 7.5-mm zirconia rotors with double bearings, and a KelF drive tip. Plugs confining the sample to the central part of the rotor were made from Teflon (HX) and boron nitride (HFX). Samples can be spun at the magic angle at spinning speeds of up to 6.7 kHz.

The double-resonance HF probe uses 4-mm rotors with Vespel drive tips and Vespel or PTFE spacers, depending on which nucleus is being observed. These rotors can be spun at up to 17 kHz, although only slow spinning speeds were required for the measurement of the spinning-sidebands (ssb). For very slow spinning speeds (below 1600 Hz), a homemade spinner tip with no flutes was used. In this case the spinning speed could not be automatically locked, but it did not drift significantly during the short run required. A ^{19}F spectrum with negligible spinning-sidebands could be obtained for both compounds at speeds above 10 kHz. The probe has an adjustable trap between the proton and fluorine channels, allowing direct fluorine observation with proton high-power decoupling.

All measurements were made at ambient temperature. The sample temperature has been calibrated using methanol/tetrakis(trimethylsilyl)silane (TTMSS) (*15*), allowing for the rotor spinning speed, and was found to be 21°C for the HF measurements and 29°C for the HX probe, with the sample spinning at 4 kHz for both probes.

Proton and fluorine powers were calibrated by finding a 180° null pulse using polydimethyldisiloxane (PDMSO) and C_6F_6 respectively. Typically, powers of 50 kHz were used. Fluorine-19 chemical shifts were referenced by replacement to liquid C_6F_6 at $\delta = -166.4$ ppm (with respect to $CFCl_3$), measured with proton high-power irradiation (so as to have the same Bloch–Siegert shift as for the proton-decoupled spectra of the tin fluorides). On the HF probe, fluorine and proton powers of ca. 80 kHz (equivalent to 3-μs 90° pulses) were employed. The proton decoupler power reaching the probe is higher than this as the cross diodes used for calibration are removed for decoupling. At these powers, the ^{19}F resonance shift due to the Bloch–Siegert effect (*14*) when proton irradiation is used during observation for decoupling is +2.3 ppm. Tin-119 RF powers were calibrated by optimising the Hartmann–Hahn match for $(C_6H_{11})_4Sn$. This compound was also used as a secondary external shift reference with $\delta = -97.4$ ppm (*16*) with respect to $SnMe_4$. Bloch–Siegert shifts are negligible for $^{119}Sn-\{^{1}H, ^{19}F\}$ NMR.

The ^{119}Sn and ^{19}F results presented here are from experiments recorded using CP from protons. Cross polarization from ^{19}F was also used for some ^{119}Sn spectra, giving closely comparable results, though the longer recycle delay necessary for ^{19}F relaxation in the compounds made ^{1}H CP preferable. For the HETCOR experiment, the $^{19}F-^{119}Sn$ Hartmann–Hahn match was optimized and found to be broad at the spinning speeds used. The pulse sequence for this experiment is shown in Fig. 1, with the optional ^{119}Sn decoupling during t_1. Individual spectrometer operating parameters are listed in the figure legends.

Spin–lattice relaxation data were measured for protons using an inversion-recovery pulse sequence, but observing the change in $^{19}F\{^{1}H\}$ magnetization after cross polarization. For ^{19}F and ^{119}Sn, the modified Torchia inversion-recovery sequence (*17*) was used, with ^{1}H decoupling during observation but not during the relaxation period τ. $T_{1\rho}$ values for ^{1}H nuclei were calculated from a spin-lock experiment with cross polarization to ^{19}F, while ^{19}F and ^{119}Sn $T_{1\rho}$ values were measured by spin-locking the magnetization after CP from ^{1}H. The ^{119}Sn magnetization could only be spin-locked for up to 20 ms because of the limitations of the amplifier. For the other nuclei, spin-lock times of up to 100 ms were used. These $T_{1\rho}$ values were then used with variable contact-time experiment results for contact times up to 10 ms to fit T_{1S}.

$^{n}Bu_3SnF$ was used as supplied by Pilkington Bros. Plc. It has an unknown impurity which is visible in the ^{119}Sn NMR

spectrum at $\delta = 121$ ppm. Mes_3SnF was donated by H. Reuter (Institut für Anorganische Chemie, Universität Bonn). Both samples are free-running white powders. They were packed into the rotors with light tamping.

Experiments were run at two different spinning speeds to confirm the position of the centerband. The spinning-sideband manifolds were analyzed using an in-house program (*18*) based on the method of Maricq and Waugh (*19*). The spinning-sideband analysis program minimizes the sum of differences squared between the experimental and calculated data to find the effective anisotropy and asymmetry. This program has been substantially modified for the present purposes in three ways:

(a) To give an estimate of the errors in fitting ζ and η (*20*). These are substantial for small asymmetries (*21*, *22*). For values of $\eta < 0.2$, there is little difference between the ssb manifolds for the nearly axial and truly axial cases.

(b) To give a triple fit of the double-decoupled and scalar-coupled spinning sideband manifolds to optimize the derivation of three effective anisotropies, in the first instance assuming coaxiality of the relevant tensors. This procedure gives an improved estimate of the effective dipolar coupling constant, D'.

(c) To relax the coaxiality condition, which was found to be necessary for the ^{119}Sn spectrum in the Mes_3SnF case but not for $^n Bu_3SnF$—in the latter case fitting without coaxiality gave $<10°$ departure from axiality, with only a marginal improvement in the sum of differences squared. In both cases, results were not sensitive to the angle β, so that only the angle α (between the Sn, F internuclear distance and σ_{33}) has been derived for Mes_3SnF.

Both peak heights and deconvoluted integral data were used and gave closely similar results. The results from the latter are given here. Directly integrated intensities were not used because of the overlap of some peaks. Throughout these simulations it has been assumed that there is no change in relative peak intensities due to cross polarization (*23*) or weak pulse losses. This was checked for the large $^n Bu_3SnF$ ^{119}Sn anisotropies by looking at the difference in calculated anisotropies between a spectrum measured by CP and one acquired using a small tip angle and direct excitation.

The definition of the shielding anisotropy $\zeta = \sigma_{33} - \sigma_{iso}$ is used herein, with the components of the tensors labeled according to $|\sigma_{33} - \sigma_{iso}| \geqslant |\sigma_{11} - \sigma_{iso}| \geqslant |\sigma_{22} - \sigma_{iso}|$. We define D' as $D - \Delta J/3$, where D is the dipolar coupling constant in frequency units, $D = (\mu_0/4\pi)\gamma_{Sn}\gamma_F(\hbar/2\pi)r_{SnF}^{-3}$ and ΔJ is the anisotropy in J, $\Delta J = J_\parallel - J_\perp$. For the spinning-sideband manifolds affected by both the relevant shielding tensor and by D' we designate the effective tensor components as σ_{ii}^{eff} and the related anisotropy and asymmetry by ζ^{eff} and η^{eff} respectively. Analysis of the spinning-sideband manifolds allows the determination of ζ and D' separately, using $\zeta^{eff} = \zeta - (2D'/\nu_0)m_x$, where ν_0 is the Larmor frequency and m_x is the appropriate spin component quantum number.

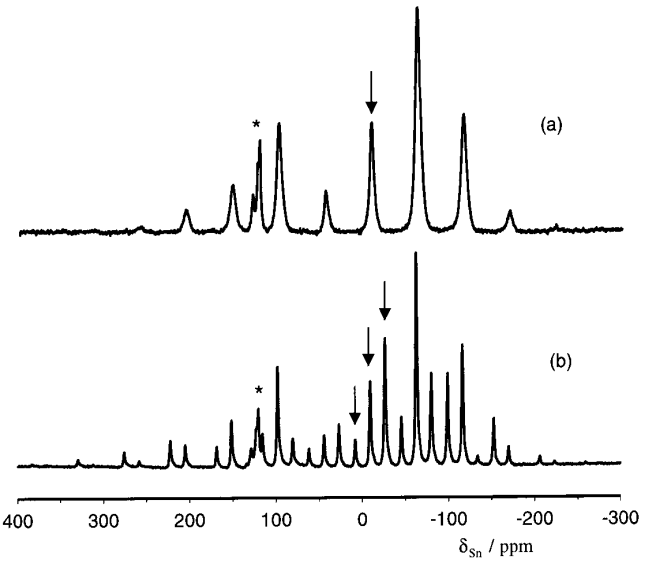

FIG. 2. Tin-119 CPMAS NMR spectra of $^n Bu_3SnF$, obtained with spinning at 4 kHz together with (a) double decoupling, and (b) only ^{1}H decoupling. The centerbands are indicated by vertical arrows. The peak marked by an asterisk at $\delta = 121$ ppm is an impurity. Acquisition parameters were: (a) pulse duration 5 μs, contact time 1 ms, recycle delay 2 s, and number of acquisitions 21,000; (b) pulse duration 5 μs, contact time 1 ms, recycle delay 2 s, and number of acquisitions 27,000.

RESULTS AND DISCUSSION

Tin-119 CPMAS spectra of $^n Bu_3SnF$ with single (proton) and double (proton and fluorine) decoupling were recorded and are shown in Fig. 2. Figure 2b shows the triplet splitting arising from isotropic coupling to two equivalent fluorine nuclei. The coupling constant is found to be $^1J(SnF) = 1310$ Hz (known to be positive (*8*)), which is naturally the same when measured from the fluorine spectrum. The peak at $\delta = 121$ ppm arises from an impurity which overlaps with two of the spinning-sideband (ssb) peaks. Thus deconvolution of the lineshape in this region has been used to get integral values of the peaks.

For the spinning-sideband simulation, all three sets of ssb were fitted together and the total sum of the differences squared was minimized. Analyses of the doubly decoupled spectrum, Fig. 2a and of one obtained at a spin rate of 2.5 kHz, confirm the centerband values. The triple fit results are shown in Table 1. Individual ssb manifold fittings gave results in agreement, within the fitting error, to the triple fit. The fit shows that the effective dipolar and chemical shift tensors are coaxial and gives a value for $D' = -3770$ Hz. A direct polarization experiment using a small pulse duration appropriate for the Ernst tip angle was carried out, giving a D' value of -3790 Hz. The values for the anisotropies are

TABLE 1

Summary of the Spinning-Sideband Analysis for $^{n}Bu_3SnF$, with Observation of ^{119}Sn at 74.63 MHz and Spinning at 4 kHz (See Fig. 2b)

δ_{iso} (ppm)	ζ^{eff} (ppm)	η^{eff}	$\sigma_{11}^{eff} - \sigma_{ref}$ (ppm)	$\sigma_{22}^{eff} - \sigma_{ref}$ (ppm)	$\sigma_{33}^{eff} - \sigma_{ref}$ (ppm)
(8.6)[a]	−332	0.0	157	157	−341
−9.0	−231	0.0	125	125	−222
(−26.7)[a]	−130	0.0	92	92	−103

[a] Values in parentheses are for the outer lines of the Sn–F coupled multiplets.

TABLE 2

Summary of the Spinning-Sideband Analysis for $^{n}Bu_3SnF$, with Observation of ^{19}F at 188.29 MHz and Spinning at 2400 Hz (See Fig. 3)

δ_{iso} (ppm)	ζ^{eff} (ppm)	η^{eff}	$\sigma_{11}^{eff} - \sigma_{ref}$ (ppm)	$\sigma_{22}^{eff} - \sigma_{ref}$ (ppm)	$\sigma_{33}^{eff} - \sigma_{ref}$ (ppm)
(−153.7)[a]	18	0.0	145	145	172
−157.0	41	0.0[b]	136	136	198
(−160.7)[a]	64	0.0	129	129	225

Note. The values in the table have been corrected for the Bloch–Siegert shift.

[a] Values in parentheses are for the Sn satellite spinning-sideband manifolds.

[b] The asymmetry found with a single fit is 0.3. The triple fit finds that $\eta = 0.0$ so this has been used.

the same within experimental error as those of the CP experiment, indicating no significant loss of intensity due to CP.

The static spectrum, recorded overnight, is dipolar broadened, and the intensity is spread over a large range, making the turning points hard to discern accurately. However, it shows axial character and $\sigma_{\perp}^{eff} - \sigma_{ref}$ values of 150, 120, and 90 ppm may be derived, in good agreement with the spinning-sideband fitted data.

The ^{19}F spectrum is shown in Fig. 3. Its spinning-sidebands, including those of the $^{117,119}Sn$ satellite peaks, have been analyzed together to give complementary information to the ^{119}Sn spectra. As the magnetogyric ratios of ^{117}Sn and ^{119}Sn are so close, satellite peaks cannot be separated for the two isotopomers. The triple fit simulation shows that the tensors are coaxial, as is the case for ^{119}Sn, and gives a value of $D' = -4340$ Hz. The results are shown in Table 2. For the centerband, $\eta = 0.3$ when calculated individually, but the triple fit gave $\eta = 0.0$. The derived anisotropy was not significantly different between the two cases.

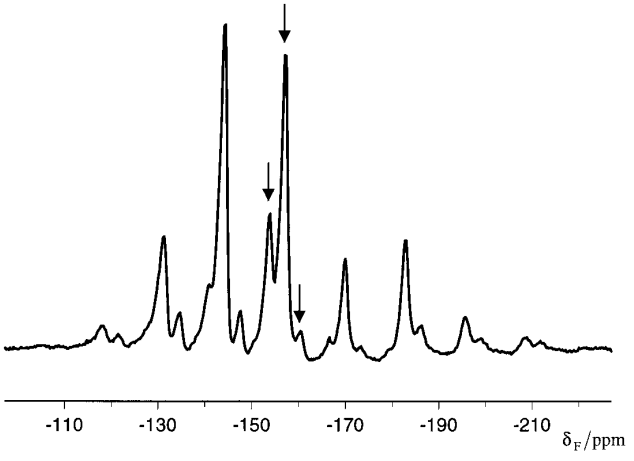

FIG. 3. Fluorine-19 CPMAS NMR spectrum of $^{n}Bu_3SnF$, obtained with spinning at 2400 Hz and proton decoupling. The centerbands are indicated by vertical arrows. The Bloch–Siegert correction of +2.3 ppm has been applied to the frequency scale. Acquisition parameters were pulse duration 3 μs, contact time 2 ms, recycle delay 3 s, and number of acquisitions 512.

Using a modified version of the fitting program, the errors in the anisotropies have been estimated to be 10%. This has the effect of a 20% error for D'. This means that for $^{n}Bu_3SnF$ that the D' values calculated by observing the two different nuclei are within experimental error. Thus the result for $^{n}Bu_3SnF$ may be quoted as $D' = -4000 \pm 400$ Hz.

The value of ΔJ could not be obtained with confidence because the Sn–F bond length is not known. However, the bond length for tribenzyltin fluoride has been measured (*24*) with two values reported to be 2.12 and 2.21 Å (equal, to within experimental error). Using these bond lengths and the average value for D', a value for ΔJ in the range +240 to −1320 Hz may be derived, which is smaller in magnitude than that for Mes_3SnF (see below), as would be expected from the smaller isotropic scalar coupling constant. A graph of ΔJ against the Sn–F bond length can be plotted as in (*8*). More accurate bond lengths need to be measured for this compound before an accurate value of ΔJ can be calculated. An *ab initio* calculation for ΔJ for Me_3SnF has been carried out (*25*) giving $\Delta J = -1770$ Hz, which compares with the previously experimentally estimated value of $\Delta J = -4020$ Hz (*8*).

The tin shielding anisotropy for $^{n}Bu_3SnF$ is consistent with the previous result of $\zeta = -207$ ppm (*6*). The asymmetry was quoted as $\eta = 0.42$, whereas the current results make the shielding tensor axial. We believe that the data here are more accurate, and that the system is indeed axial. Results for other penta-coordinate trigonal bipyramidal fluorine-bridged compounds have values for the anisotropy lying between −200 and −255 ppm. SA values for trigonal bipyramidal compounds of tin with C_3O_2 and C_3N_2 nearest neighbors are similar in magnitude and are also negative (*26–28*).

The ^{119}Sn spectra of Mes_3SnF in Fig. 4 show splittings arising from scalar isotropic coupling to both fluorine and carbon with average $^{1}J(SnF) = 2275$ Hz and $^{1}J(SnC)$ of about (−)550 Hz (indicated by a dagger in Fig. 4b), with the doubly decoupled spectrum unambiguously confirming

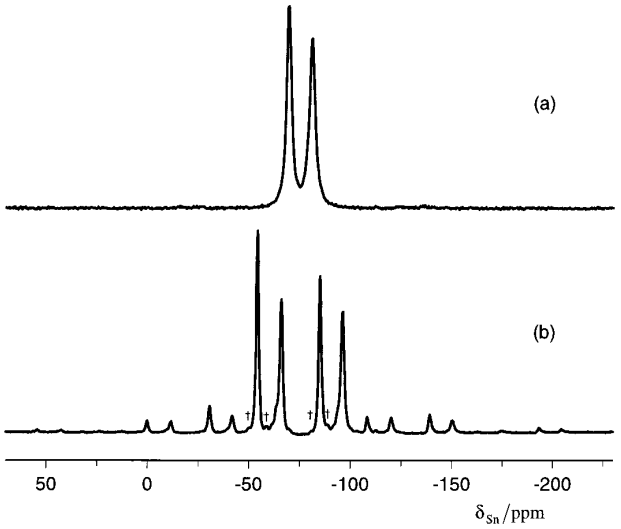

FIG. 4. Tin-119 CPMAS NMR spectra of Mes_3SnF, obtained with spinning at 4 kHz together with (a) double decoupling, and (b) only ^1H decoupling. The weak ^{13}C satellites are marked by a dagger. Acquisition parameters were: (a) pulse duration 4 μs, contact time 4 ms, recycle delay 3 s, and number of acquisitions 1256; (b) pulse duration 5 μs, contact time 5 ms, recycle delay 5 s, and number of acquisitions 9045.

the assignment of the splitting caused by coupling to ^{19}F (reinforcing earlier variable-field experiments (*7*)). The sign of $^1J(SnC)$ is known to be negative by analogy to similar couplings in Me_4Sn (*29*).

By contrast to $^nBu_3SnF$, Mes_3SnF has small ^{119}Sn effective anisotropies, so the spectra show few spinning-sidebands with significant intensity. This is especially true for doubly decoupled spectra, showing that D' is substantially larger in magnitude than the true shielding anisotropy. As there are also two molecules in the asymmetric unit, the spectrum cannot be easily interpreted when recorded at a slow spinning speed as it becomes too cluttered. This results in few ssb's which leads to poorly defined anisotropies. However, a proton-decoupled spectrum has been recorded with the sample spinning at 2 kHz. At this speed the peaks are interleaved, so that useful information can be obtained by careful deconvolution. There are still only two spinning-sidebands, but their intensities are much greater, giving a better signal-to-noise ratio and thus a smaller error. A combined fit of the three sets of data, two from the singly decoupled and one from the doubly decoupled spectrum (recorded at the same spin rate), has been performed, with the results summarized in Table 3. The double decoupling is particularly significant for the measurement of the shielding anisotropies, free from the effects of D'. In this case, when the system is treated as coaxial, the anisotropies are found to be 12 and 1 ppm for the two sites, whereas when this condition is relaxed, they are obtained as 12 and 19 ppm. This indicates that the tensors are not coaxial. The triple fit shows that site 1 appears to be almost colinear, with $D' = -4690$ Hz. However, for site 2 the shielding tensor is tilted by approximately 50° from the dipolar tensor. For this site, the effective dipolar tensor is $D' = -4500$ Hz, compared with -4720 Hz if colinearity is assumed.

The ^{19}F NMR spectrum of Mes_3SnF is shown in Fig. 5. The centerband peaks are indicated by vertical arrows and the low-frequency satellite peaks by daggers. The high-frequency satellite peaks are too weak to be visible. Two-dimensional HETCOR spectra measured with the sample spinning at 4 kHz, with direct observation of the ^{119}Sn and indirect observation of the ^{19}F, are shown in Fig. 6. The contact time is very short (0.3 ms), allowing only transfer of ^{19}F magnetization to nearby nuclei. Figure 6a shows the ^{19}F spectrum in ω_1 for fluorines directly bonded to ^{119}Sn. This is equivalent to the tin satellite peaks in the normal ^{19}F spectrum (Fig. 5). For comparison, Fig. 6b has ^{119}Sn decoupling on during t_1 so that the ω_1 spectrum is equivalent to the ^{19}F spectrum without the satellite peaks present. These spectra clearly show the two sites in the asymmetric unit with their ^{19}F and ^{119}Sn chemical shifts correlated. These values are given in Tables 3 and 4.

For spinning-sideband analysis of the ^{19}F spectrum, the satellite peaks have little intensity and lie on the shoulders

TABLE 3

Summary of the Spinning-Sideband Analysis for Mes_3SnF, with Observation of ^{119}Sn at 74.63 MHz and Spinning at 2 kHz Using Simultaneous Fitting of the Singly and Doubly Decoupled Cases, Spectra Not Shown

	δ_{iso} (ppm)		ζ^{eff} (ppm)	η^{eff}	$\sigma_{11}^{eff} - \sigma_{ref}$ (ppm)	$\sigma_{22}^{eff} - \sigma_{ref}$ (ppm)	$\sigma_{33}^{eff} - \sigma_{ref}$ (ppm)
		(−54.0)[a]	−51	0.2	85	74	3
Site 1	−69.2		12	0.9	58	69	81
		(−84.8)[a]	75	0.1	42	53	160
		(−65.9)[a]	−62	0.3	107	87	3
Site 2[b]	−80.6		19	0.1	70	72	100
		(−96.0)[a]	63	0.3	55	74	159

[a] Values in parentheses are for the outer lines of the Sn−F coupled multiplets.

[b] In this case nonaxiality between the dipolar and shielding tensors was found (see the text).

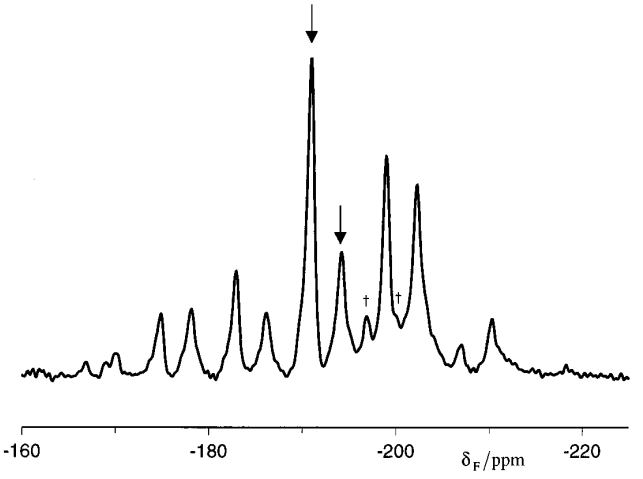

FIG. 5. Fluorine-19 CPMAS NMR spectrum of Mes_3SnF, obtained with spinning at 1505 Hz together with proton decoupling. The centerbands are indicated by vertical arrows, and the low frequency satellites are marked by a dagger. The Bloch–Siegert correction of +2.3 ppm has been applied to the frequency scale. Acquisition parameters were pulse duration 3 μs, contact time 5 ms, recycle delay 3 s, and number of acquisitions 64.

of the main peaks. This makes their intensity hard to measure, even by deconvolution. However, a 2D HETCOR experiment run at 1500 Hz separates the two sites and leaves only the ^{119}Sn satellite peaks. The two satellite peaks to low frequency turn out to have values of ζ^{eff} near zero, giving single peaks at $\delta = -196.8$ and -200.1 ppm. The high-frequency satellites have larger effective anisotropies, so their intensities are spread over a number of spinning-sidebands, giving many low-intensity peaks.

A triple fit of the centerband, for the 1D spectrum, and satellite peaks, for the 2D spectrum, spinning-sideband manifolds has been performed. This allows approximate values for ζ^{eff} to be calculated. The error in these values is large due to the poor signal-to-noise ratio. Using these values gives the effective dipolar coupling constant as $D' = -3420$ Hz (site 1) and -4290 Hz (site 2). The triple fit simulation shows that the two tensors are probably coaxial, although the data used here are not well defined. The errors in D' are large, though the differences between the two sites are possibly significant. The values are smaller than that found for ^{119}Sn, but are reasonable considering the large errors in the ^{19}F and ^{119}Sn measurements.

The Mes_3SnF SA is much smaller than that for $^{n}Bu_3SnF$ (in fact only just measurable). The previous results (*8*) are hard to compare as they were measured at 111.86 MHz. The crystal structure shows distorted C_{3v} symmetry, so a nonzero asymmetry would be expected. We believe the present data are the more accurate, since they are produced by simultaneous fitting of three spinning-sideband manifolds. Moreover, the present work succeeded in recording the ^{119}Sn ssb pattern at a much slower spinning speed by interleaving the peaks and careful deconvolution. Thus the outlying peaks have improved signal-to-noise ratios, which increases the accuracy of the results. However, it is clear that, because of the low values of the anisotropies (which are much lower in magnitude than the dipolar coupling constants), there are considerable uncertainties in the results for Mes_3SnF.

For Mes_3SnF an X-ray diffraction measurement has been made that gives the Sn–F bond lengths as 1.957 and 1.965 Å (*30*). Recalling that the magnetogyric ratio for ^{119}Sn is negative gives $D = -5650$ and -5582 Hz for the two bond lengths respectively. Using $D' = -4600$ Hz allows one to calculate $\Delta J = -3150$ and -2950 Hz (for the two molecules in the asymmetric unit), although it is not possible to say which values of ΔJ and bond length correlate to which particular chemical shift. The errors in calculating ΔJ are

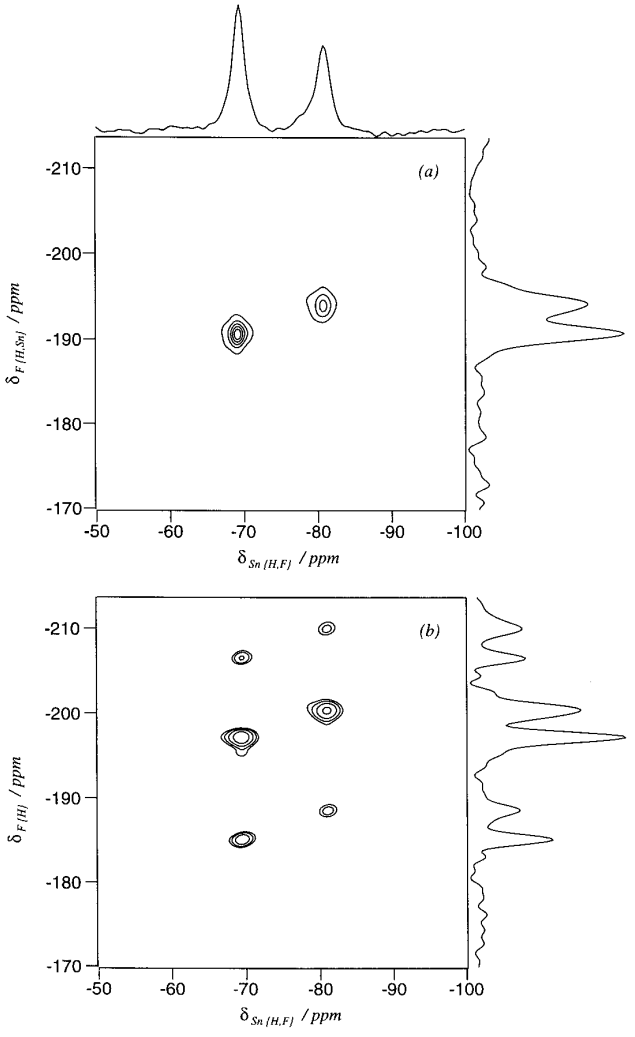

FIG. 6. Two-dimensional heteronuclear correlation spectra obtained by observing ^{119}Sn {^{1}H, ^{19}F} in t_2 and (a) ^{19}F {^{1}H, ^{119}Sn}, (b) ^{19}F {^{1}H} in t_1. The pulse sequence is shown in Fig. 1. Acquisition parameters were: (a) ^{19}F transmitter frequency 188.275 MHz, pulse duration 5 μs, dwell (t_1) 100 μs, points in t_1 32, zero-filled to 256, contact time 0.3 ms, recycle delay 10 s, and number of acquisitions per slice 16; (b) ^{19}F transmitter frequency 188.275 MHz, pulse duration 5 μs, dwell (t_1) 100 μs, points in t_1 64, zero-filled to 256, contact time 0.3 ms, recycle delay 10 s, and number of acquisitions per slice 64.

TABLE 4
Summary of the Spinning-Sideband Analysis for Mes_3SnF, with Observation of ^{19}F at 188.29 MHz and Spinning at 1505 Hz (See Fig. 5)

	δ_{iso} (ppm)		ζ^{eff} (ppm)	η^{eff}	$\sigma_{11}^{eff} - \sigma_{ref}$ (ppm)	$\sigma_{22}^{eff} - \sigma_{ref}$ (ppm)	$\sigma_{33}^{eff} - \sigma_{ref}$ (ppm)
		(−185.0)[a]	−36	0.3	209	198	149
Site 1	−190.9		−18	0.6	205	195	173
		(−196.8)[a]	6	0.5	192	195	203
		(−188.3)[a]	−49	0.2	218	207	139
Site 2	−194.2		−26	0.4	213	202	168
		(−200.1)[a]	7	0.0	196	196	208

Note. The satellite spinning-sideband manifolds used were from a 2D HETCOR experiment similar to Fig. 6(a) but spinning at 1500 Hz. The values in the table have been corrected for the Bloch–Siegert shift.

[a] Values in parentheses are for the outer lines of the Sn–F coupled multiplets.

significant, especially due to the small magnitudes of the true shielding anisotropies, so the two values given above cannot be distinguished experimentally.

In general, as the coordination number (CN) of the tin center increases from four (Mes_3SnF) to five ($^nBu_3SnF$) the isotropic ^{119}Sn chemical shift would be expected to decrease (i.e., the tin nucleus should become more shielded), but the reverse is observed in the present case. However, the organic group also affects the shielding strongly, with aromatic groups deshielding the tin nucleus relative to aliphatic groups. This is confirmed by Ph_3SnF, which has a similar organic group to mesityl but is penta-coordinate and has $\delta = -211.9$ ppm (*7*), i.e., approximately 140 ppm to low frequency of the shift for Mes_3SnF, confirming the effect of coordination number.

Though the SnF bond lengths for $^nBu_3SnF$ are unknown, they would be expected to be in the range 2.1–2.3 Å by analogy with the similar compound $benzyl_3SnF$ (*24*). However, Mes_3SnF has shorter bond lengths of 1.96 Å (*30*). This manifests itself in the isotropic coupling constants, where the longer bond length and bridging in $^nBu_3SnF$ give a value that is almost half those for Mes_3SnF. The magnitude of ΔJ is also larger for the latter, i.e., in line with the isotropic J values, as might be expected.

Relaxation data are summarized in Table 5 for both compounds. The longitudinal relaxation times, T_1, of ^{19}F and ^{119}Sn for Mes_3SnF are longer than those for $^nBu_3SnF$, implying reduced motion in the Mes_3SnF system. The values of T_1 (^1H) for both compounds are short. Spin-locked, $T_{1\rho}$, relaxation for Mes_3SnF is long for all nuclei studied and could not be determined for ^{19}F. For $^nBu_3SnF$, $T_{1\rho}$ (^1H) is small and similar in size to T_{HSn}, so the extended cross-polarization equation given by Mehring (*31*) is necessary to describe the variable contact-time experiment. This gives a good fit to the experimental data, also agreeing with the direct $T_{1\rho}$ measurement, and was used to calculate T_{HSn}. The relative intensity of ^{119}Sn signals given by cross polarization (from ^1H) and those from direct polarization spectra for $^nBu_3SnF$ show an eightfold improvement for the former at constant time.

Use of the HFX probe with double decoupling of both ^1H and ^{19}F simplifies the spectra, as can be seen in Fig. 4a for Mes_3SnF. This is also the case for $^nBu_3SnF$, for which the doubly decoupled spectrum is shown in Fig. 2a. For Mes_3SnF, varying the ^{19}F decoupler power leads to a change in the spectrum, Fig. 7, which can be explained as arising from decoupling off-resonance. The effective coupling between ^{119}Sn and ^{19}F is dependent on both the power and the offset of the ^{19}F decoupling field (*32*), as given in Eq. [1], where B_2 is the decoupler field strength, $\delta\nu$ is the offset of irradiation from ^{19}F resonance, and J_r is the reduced splitting.

$$\left(\frac{\gamma}{2\pi}\right)B_2 = \delta\nu\,\frac{\sqrt{J^2 - J_r^2}}{|J_r|}. \qquad [1]$$

Figure 8 shows the reduced splitting when the decoupler is offset from 188.29 MHz, its usual position in our operations. The most efficient decoupling, when on resonance, can be seen to occur with an offset of 10.5 kHz from this frequency. Using

TABLE 5
Summary of the Relaxation Data Obtained for $^nBu_3SnF$ and Mes_3SnF

Parameter	$^nBu_3SnF$	Mes_3SnF
$T_1(^1H)$ (s)	1.5	1.1
$T_1(^{19}F)$ (s)	3.4	7.5
$T_1(^{119}Sn)$ (s)	13	29/51[b]
$T_{1\rho}(^1H)$ (ms)	1.9	58[a]
$T_{1\rho}(^{19}F)$ (ms)	3.4	Long[a]
$T_{1\rho}(^{119}Sn)$ (ms)	12	700/1000[a,b]
T_{HF} (ms)	0.4	0.4
T_{HSn} (ms)	0.6	0.5

[a] For such long $T_{1\rho}$ values, only the initial gradient could be measured.

[b] For the two sites at $\delta = -69.2$ and -80.6 ppm respectively.

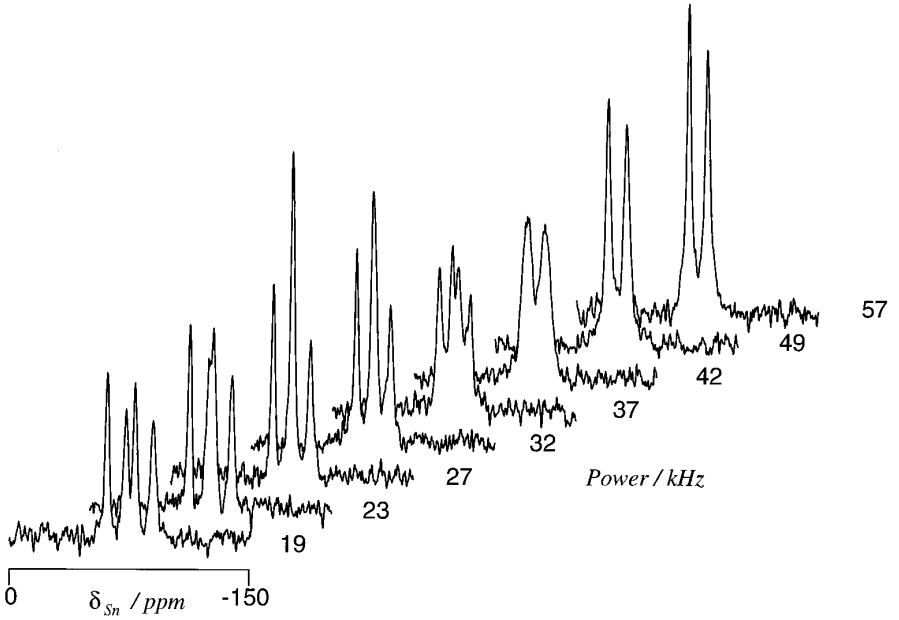

FIG. 7. Tin-119 CPMAS NMR spectra of Mes_3SnF, obtained with spinning at 4 kHz together with proton decoupling and variable-power ^{19}F decoupling. These powers were calibrated by measuring 90° pulse durations on C_6F_6 and are given in kHz beside each spectrum. The ^{19}F decoupler was offset by 10.5 kHz from the centerband resonance as measured from Fig. 8. Acquisition parameters were pulse duration 4 μs, contact time 5 ms, recycle delay 5 s, and number of acquisitions 8. The ^{19}F power was adjusted manually.

this value for $\delta\nu$, the decoupling powers can then be calculated from the spectra in Fig. 7 by measuring the value of J_r for each slice. This is consistent with those powers found from 90° pulse duration experiments and produces a quick and accurate method to calibrate the decoupler powers. Another advantage of reduced splittings is to simplify the spectrum without fully removing the coupling, which can give valuable information e.g., on multiplicities in crowded spectra.

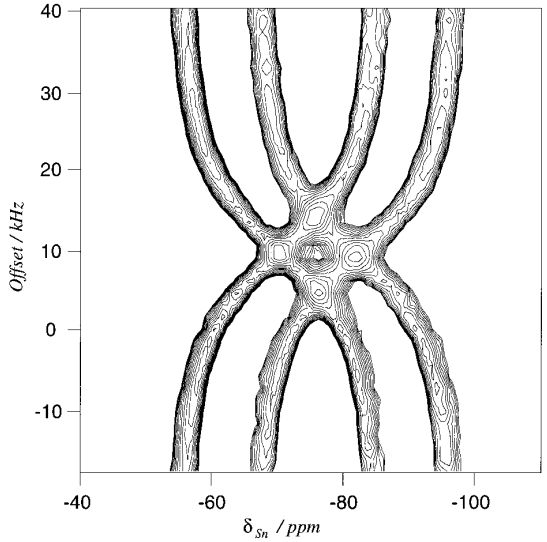

FIG. 8. Contour plot of tin-119 CPMAS NMR spectra of Mes_3SnF, obtained with spinning at 4 kHz together with proton decoupling and variable-offset ^{19}F decoupling. Acquisition parameters were pulse duration 4.5 μs, contact time 4 ms, recycle delay 3 s, and number of acquisitions 32.

CONCLUSIONS

It has been demonstrated that both ^{119}Sn and ^{19}F spectra of the compounds $^{n}Bu_3SnF$ and Mes_3SnF may be used for the calculation of D', as well as shielding tensor components, although use of the ^{119}Sn spectra is better as there is not the necessity to analyze weak $^{117,119}Sn$ satellite peaks. The finding of zero effective asymmetry for $^{n}Bu_3SnF$ supports our assumption that this system can be reasonably treated as having coaxial shielding, dipolar, and indirect coupling tensors. However, for Mes_3SnF, the tensors do not appear to be coaxial. Use of the new HFX probe for double decoupling of ^{1}H and ^{19}F gives higher resolution spectra and opens up new experimental possibilities. Cross polarization from ^{19}F to ^{119}Sn has been successful and was used to measure ^{19}F–^{119}Sn heteronuclear correlation spectra of Mes_3SnF.

ACKNOWLEDGMENTS

We are grateful to the U.K. Engineering and Physical Sciences Research Council for a research studentship for one of us (J.C.C.) and for Research Grants GR/H96096 and GR/J97557, which provided finances for the purchase of the Chemagnetics spectrometer. One of us (J.C.C.) thanks I.C.I. for a scholarship. We thank Dr. A. Minoja for some preliminary ^{19}F experiments.

REFERENCES

1. R. K. Harris, A. Sebald, D. Furlani, and G. Tagliavini, *Organometallics* **7,** 388 (1988).

2. D. C. Apperley, N. A. Davies, R. K. Harris, S. Eller, P. Schwarz, and R. D. Fischer, *J. C. S. Chem. Commun.* **10,** 740 (1992).
3. R. K. Harris and A. Sebald, *Magn. Reson. Chem.* **27,** 81 (1989).
4. T. B. Grindley, R. E. Wasylishen, R. Thangarasa, W. P. Power, and R. D. Curtis, *Can. J. Chem.* **70,** 205 (1992).
5. R. K. Harris, S. E. Lawrence, S. Oh, and V. G. Kumar Das, *J. Mol. Struct.* **347,** 309 (1995).
6. R. K. Harris, K. J. Packer, and P. Reams, *Chem. Phys. Lett.* **115,** 16 (1985).
7. H. P. Bai, R. K. Harris, and H. Reuter, *J. Organomet. Chem.* **408,** 167 (1991).
8. H. P. Bai and R. K. Harris, *J. Magn. Reson.* **96,** 24 (1992).
9. S. A. Carss, R. K. Harris, P. Holstein, B. J. Say, and R. A. Fletton, *J. C. S. Chem. Commun.* **20,** 2407 (1994).
10. S. A. Carss, U. Scheler, R. K. Harris, P. Holstein, and R. A. Fletton, *Magn. Reson. Chem.* **34,** 63 (1996).
11. R. K. Harris, S. A. Carss, R. D. Chambers, P. Holstein, A. P. Minoja, and U. Scheler, *Bull. Magn. Reson.* **17,** 37 (1996).
12. E. W. Hagaman, *J. Magn. Reson. A* **104,** 125 (1993).
13. E. W. Hagaman and J. H. Burns, *Fuel* **72,** 1239 (1993).
14. S. A. Vierkötter, *J. Magn. Reson. A* **118,** 84 (1996).
15. A. E. Aliev and K. D. M. Harris, *Magn. Reson. Chem.* **32,** 366 (1994).
16. R. K. Harris and A. Sebald, *Magn. Reson. Chem.* **25,** 1058 (1987).
17. D. A. Torchia, *J. Magn. Reson.* **30,** 613 (1978).
18. J. R. Ascenso, L. H. Merwin, and H. Bai, ''In-house Sideband Fitting Program,'' University of Durham.
19. M. M. Maricq and J. S. Waugh, *J. Chem. Phys.* **70,** 3300 (1979).
20. A. C. Olivieri, *J. Magn. Reson. A* **123,** 207 (1996).
21. N. J. Clayden, C. M. Dobson, L. Lian, and D. J. Smith, *J. Magn. Reson.* **69,** 476 (1986).
22. R. K. Harris, P. Jackson, L. H. Merwin, B. J. Say, and G. Hägele, *J. C. S. Faraday 1* **84,** 3649 (1988).
23. G. Jeschke and G. Grossmann, *J. Magn. Reson. A* **103,** 323 (1993).
24. H. Reuter, Doctoral Thesis, University of Bonn (1987).
25. G. A. Aucar, personal communication.
26. D. C. Apperley, N. A. Davies, R. K. Harris, A. K. Brimah, S. Eller, and R. D. Fischer, *Organometallics* **9,** 2672 (1990).
27. J. Kummerlen, A. Sebald, and H. Reuter, *J. Organomet. Chem.* **427,** 309 (1992).
28. J. Kummerlen and A. Sebald, *J. Am. Chem. Soc.* **115,** 1134 (1993).
29. W. McFarlane, *J. Chem. Soc. (A),* 528 (1967).
30. H. Reuter and H. Puff, *J. Organomet. Chem.* **379,** 223 (1989).
31. M. Mehring, Principles of high resolution NMR in solids, *in* ''NMR—Basic Principles and Progress'' (J. S. Waugh, Ed.), Vol. 12, p. 282, Springer-Verlag, Berlin/New York (1983).
32. A. E. Derome, ''Modern NMR Techniques for Chemistry Research,'' p. 158, Pergamon Press, Oxford (1987).